

Symmetries of CMB Temperature Correlation at Large Angular Separations

RAY HAGIMOTO,^{1,2} CRAIG HOGAN,^{2,3} COLLIN LEWIN,^{4,2} AND STEPHAN S. MEYER²

¹*University of Texas at San Antonio*

²*University of Chicago, 5640 South Ellis Ave., Chicago, IL 60637*

³*Fermi National Accelerator Laboratory, Batavia, IL 60510*

⁴*Steward Observatory, University of Arizona, 933 North Cherry Avenue, Tucson, AZ 85721*

Submitted to ApJL

ABSTRACT

A new analysis is presented of the angular correlation function $C(\Theta)$ of cosmic microwave background (CMB) temperature at large angular separation, based on published maps derived from *WMAP* and *Planck* satellite data, using different models of astrophysical foregrounds. It is found that using a common analysis, the results from the two satellites are very similar. In particular, it is found that previously published differences between measured values of $C(\Theta)$ near $\Theta = 90^\circ$ arise mainly from different choices of masks in regions of largest Galactic emissions, and that demonstrated measurement biases are reduced by eliminating masks altogether. Maps from both satellites are shown to agree with $C(90^\circ) = 0$ to within estimated statistical and systematic errors, consistent with an exact symmetry predicted in a new holographic quantum model of inflation.

1. INTRODUCTION

In the standard cosmological model, initial conditions are set by a combination of a uniform inflationary background space-time, and perturbations from fluctuations of a quantum field vacuum matched to linearized gravity. For an appropriate choice of background parameters, the model leads to a perturbation power spectrum in good agreement with measurements of cosmic large scale structure, and with the angular spectrum of anisotropy in the cosmic microwave background radiation (CMB) (Bennett et al. 2013; Akrami et al. 2018).

Recently, a new class of models has been proposed for the quantum mechanics of inflationary initial conditions (Banks & Fischler 2018; Hogan 2019a,b). In these holographic or “spooky” models, the quantum system is based not on fields, but on coherent states of space-time structure. Quantum field states collapse coherently on comoving spatial hypersurfaces, but holographic quantum-geometrical states collapse coherently on the inflationary horizon — the inbound null cone that arrives at an observer at the end of inflation. Nonlocal entanglement leads to emergent classical scalar curva-

ture perturbations with new correlations in direction, and over a range of comoving scales.

The new approach is motivated by holographic, emergent theories of quantum gravity, in which space, time, gravity, and perhaps locality itself emerge statistically from a holographic quantum system based on null surfaces, such as light cones and horizons (Jacobson 1995; Padmanabhan 2014; Jacobson 2016). Coherent quantum horizons have been extensively studied in the contexts of black holes (’t Hooft 2016a,b, 2018; Solodukhin 2011) and anti-de Sitter spaces (Ryu & Takayanagi 2006b,a; Natsuume 2015). Quantum fluctuations of the emergent null surfaces in such theories can be much larger than the Planck-length variance predicted by standard linearized gravity, based on effective field theory; their effects on macroscopic scales might even produce detectable effects in laboratory experiments (Hogan 2017; Hogan et al. 2017; Verlinde & Zurek 2019).

In holographic inflation, coherent quantum-geometrical fluctuations of the horizon are the main source of cosmic scalar curvature perturbations (Hogan 2019a). The scaling of emergent scalar curvature perturbations produces the same nearly-scale-invariant, slightly tilted power spectrum as the standard scenario, so it duplicates every result of standard cosmology that only depends on the power spectrum. The model leads to specific predictions: an inflationary expansion rate

in Planck units given approximately by the observed scalar perturbation amplitude $Ht_P \approx A_S \approx 2 \times 10^{-9}$; a similar value for the tensor-to-scalar ratio r ; an inflationary potential with a derivative given by approximately the inverse Planck mass; and a small or vanishing intrinsic dipole and global mean curvature. The most conspicuous observable signature is that nonlocal phase correlations of primordial curvature lead to a distinctive pattern of relic cosmic large scale structure and CMB anisotropy, the subject of this work.

1.1. Predicted pattern from holographic inflation

The holographic absence of one independent degree of freedom creates new symmetries in directional relationships of the primordial potential around any observer, associated with causal constraints on primordial information (Hogan 2019b). The new symmetries are predicted to appear today as precise constraints on angular correlations that limit the range of possible patterns of CMB anisotropy. In contrast, the ensemble of possible skies in the standard quantum inflation model, based on independent random fluctuations in modes of a quantum field vacuum, includes many realizations incompatible with holographic symmetries. The holographic symmetries may enable a unified interpretation of some features in the pattern of large angle CMB anisotropy long known to disagree with expectations in the standard scenario (Bennett et al. 2011; Schwarz et al. 2016; Ade et al. 2016; Akrami et al. 2019).

In particular, emergent holographic correlations lead to new symmetries of the CMB temperature two-point correlation function,

$$C(\Theta) \equiv \langle \delta T_a \delta T_b \rangle_{\angle ab = \Theta},$$

the all-sky average of the product $\delta T_a \delta T_b$ of CMB temperature deviations from the overall mean of a dipole-subtracted map, for all pairs of points a, b at angular separation $\angle ab = \Theta$.

The most robust prediction of holographic inflation is that $C(\Theta)$ *exactly vanishes at* $\Theta = 90^\circ$, which follows simply from the independence of primordial perturbations along axes in orthogonal directions. As discussed below, this symmetry is *not* a property of the standard scenario. The prediction $C_{90} \equiv C(90^\circ) = 0$ for primordial curvature should be preserved in the observed sky temperature anisotropy: it is not affected by the magnitude or direction of any unmeasured intrinsic cosmic dipole, or by post-inflation effects that modify the distribution of temperature on small angular scales from the pattern of primordial scalar curvature; for example, it is not changed by integrated Sachs-Wolfe anisotropy, or by Doppler contributions to temperature anisotropy.

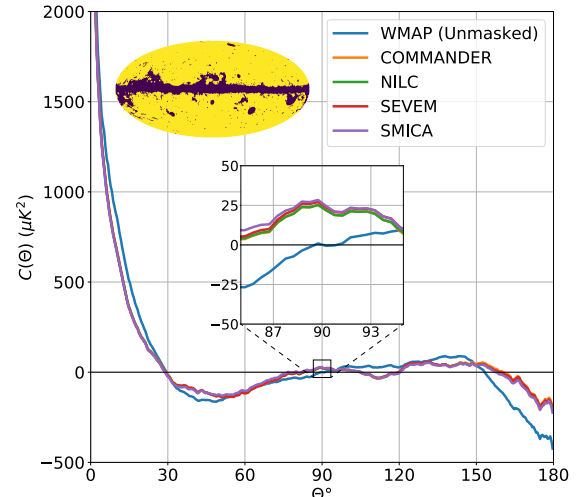


Figure 1. Comparison of *Planck* and WMAP $C(\Theta)$ functions. The lines show our recalculation of $C(\Theta)$. To make these plots, the *Planck* maps were made omitting regions of sky in the “strong” mask shown in the upper left, and the WMAP map was unmasked. These plots approximately reproduce the respective published *Planck* and WMAP correlation functions (Bennett et al. 2011; Ade et al. 2016). The inset shows a blow-up of the region centered at $\Theta = 90^\circ$, showing an apparent disagreement between *Planck* and WMAP correlation functions, and a good agreement of all four *Planck* pipelines. We have traced the bulk of this disagreement to the use of different foreground masks. When all the foreground-reduced maps from *Planck* and *WMAP* are analyzed with the same masks, the differences in the values of $C(\Theta)$ are very much reduced.

A similar causal symmetry may also lead to a nearly-vanishing correlation at $\Theta = 30^\circ$, although in this case a primordial directional symmetry of curvature is not exactly preserved by temperature anisotropy. It is also possible that the quantum states of the inflationary horizon display an antipodal antisymmetry similar to black hole horizons, in which case it should generically produce significant fine-grained anticorrelation at angles approaching 180° .

1.2. Previous analysis

While $C(\Theta)$ is well known to have small values at large angular separation (Bennett et al. 2003, 2011; Ade et al. 2016; Akrami et al. 2019), there has not been particularly close scrutiny of its exact value, both because little particular significance is attributed to them in standard cosmology, and because structure is contaminated by astrophysical emission correlated on large angular scales. A more accurate analysis of $C(\Theta)$ is needed to test predictions of an exact or nearly-exact symmetry.

The WMAP team and the *Planck* collaboration have both published papers on the correlation function and

related large angular scale statistics. The most detailed study of the *WMAP* correlation function, based on 7 years of data, includes a comparison with a standard-inflation ensemble prediction (Bennett et al. 2011). For *Planck*, temperature anisotropy and statistics for the full data set are analyzed in Ade et al. (2016); Fig. 2 in that paper shows the correlation function for the four *Planck* pipelines, made with a common mask.

In plots of $C(\Theta)$ in Ade et al. (2016), all of the *Planck* maps appear to agree with each other, but on close examination they disagree in detail with the published *WMAP* plot found in Bennett et al. (2011). We reproduce the previous results with our reanalysis of masked maps as displayed in Fig. 1. We were led to undertake the present study by the prediction $C_{90} = 0$ of holographic inflation, which appears to be inconsistent with the *Planck* measurement.

In this Letter, we describe a new uniform analysis of these maps to make an improved estimate of the cosmological correlation, particularly at $\Theta = 90^\circ$ and $> 160^\circ$. We present a comparison of $C(\Theta)$ for all the maps with uniform pixelation, smoothing, binning and masking.

2. DATA

Our analysis is based on public data releases of foreground-corrected maps of the CMB temperature from the *WMAP* and *Planck* satellites. These are the highest quality data available with consistent and homogeneous full sky coverage.

In the case of *WMAP*, we use the nine-year, Internal Linear Combination (ILC) map. This map is a reconstruction of the thermal CMB sky, separated from foreground components using multiband frequency information (Bennett et al. 2013).

In the case of *Planck*, there are four separate pipelines, using different foreground models, priors, and statistical methods: Commander, NILC, SEVEM, and SMICA. Initial results were described by Planck Collaboration (2014); both data and methods were later updated, including the full mission dataset for temperature anisotropy (Planck Collaboration 2016a). The updates of the four maps (Planck Collaboration 2016b) are adopted here.

The foreground models use a broad range of complementary assumptions and statistical approaches, with different biases. The analyses are mostly independent, but there are caveats: for example, the Commander model used some external data at low frequencies, including ground-based 408 MHz data and *WMAP* itself, so it is not entirely independent of *WMAP*; at the same time, the model was created independently of the *WMAP* ILC, and uses new *Planck* data over a wider

range of frequencies. Regarding the four *Planck* maps, we quote from (Planck Collaboration 2016a): “we generally consider Commander to be the preferred solution on large and intermediate angular scales ... [and] we confirm our preference for the SMICA map for analyses that require full-resolution observations in temperature.”

3. METHOD

To calculate $C(\Theta)$ we used the python wrapper for the Hierarchical Equal Area isoLatitude Pixelization (*HEALPix*) scheme (Gorski et al. 2004), to read in the appropriate FITS CMB map (either *WMAP*, or one of the four *Planck* pipelines) downgraded to a resolution defined by $N_{\text{side}} = 128$. We then directly computed the pairwise temperature products $\delta T_a \delta T_b$ and angular separations $\angle ab$, storing the values in an array so that each row contained $(\angle ab, \delta T_a \delta T_b)$ as an element. Masking was accomplished by skipping over any point where a or b was in the mask. Next, we found all entries for angular separations in a bin size of 0.5° , taking the angular separation Θ as the mean of the $\angle ab$ in the bin, and the unweighted mean of the corresponding $\delta T_a \delta T_b$ as the value for $C(\Theta)$. As a check of pixelation errors, $C(\Theta)$ was measured with each unmasked map for 20 random orientations. The resulting spread in all cases is less than $\pm 1 \mu\text{K}^2$.

To investigate the effect of masking on the correlation function we chose a “weak” mask and a “strong” mask from the second *Planck* public release database¹. Systematic errors introduced by foreground masks are estimated by randomly rotating the weak and strong masks. In these tests, one map, SEVEM, appears as an outlier compared with the other maps. The simplest interpretation of why the SEVEM map appears as an outlier is that it includes a larger residue of foreground contamination than the others. A visual inspection of the SEVEM map indeed shows much more emission aligned with features in the Galaxy than the other maps.

Excluding SEVEM, at $\Theta = 90^\circ$, weak masking introduces a variation range of $\sim \pm 6.5 \mu\text{K}^2$ and strong masking introduces a variation range of $\sim \pm 27 \mu\text{K}^2$. This range of variation provides an estimate of the effect on the measured value of C_{90} typically produced in each map by masking alone.

In Fig. 2, we show a comparison of the five maps with uniform weak masks and no masks near 90° . Consistent

¹ The masks are shown in as insets in Fig. 1 and Fig. 2. File-names are COM_CMB_IQU-nilc-field-Int_2048_R2.01_full and COM_CMB_IQU-common-field-MaskInt_2048_R2.01 for the weak and strong masks respectively.

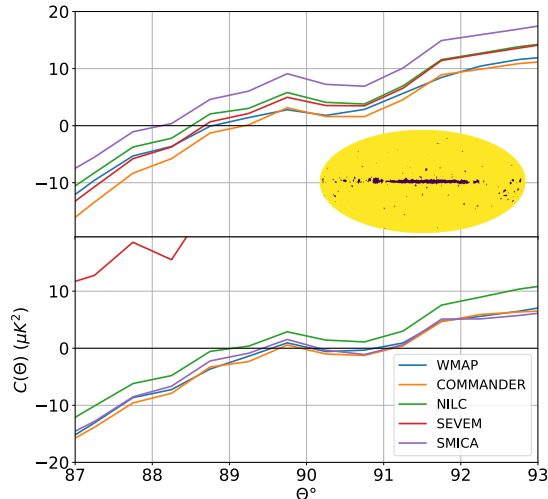


Figure 2. Estimate of the effect of masking near $\Theta = 90^\circ$. The top panel shows the $C(\Theta)$ of the four *Planck* maps and the WMAP ILC map, made with a weak mask (as shown in the inset); the four *Planck* maps now agree with WMAP, and with each other. The bottom panel shows the 5 functions with no masking. With the exception of the SEVEM map, the agreement is much tighter. The overall agreement between maps increases as the mask is reduced and then eliminated.

with the test just described, a weak mask as shown substantially reduces the variation from the comparison between WMAP and *Planck* shown in Fig. 1. Not masking at all reduces the variation between the maps still further, for all of the maps except SEVEM. It is important to note that the “no mask” maps are based on model restorations (or “inpainting”) that interpolate over small regions at the Galactic center and inner Galactic plane. The small-scale additions, to the extent that they are made independently for the different maps, seem to influence $C(\Theta)$ very little near 90° .

A closer view of $C(\Theta)$ for the foreground-subtracted, unmasked maps is shown in Fig. 3. At this level of scrutiny, an additional systematic uncertainty appears from monopole and dipole harmonics present in the WMAP ILC, which are much larger than in the *Planck* maps. The presence of a monopole is incompatible with a δT map. As shown in Fig. 3, its removal reduces the value of C_{90} by $\sim 6.7\mu K^2$, outside the range of the *Planck* maps.

The overall agreement between the different $C(\Theta)$ ’s constrains both independent statistical and independent systematic errors in the measurements, although any in-common systematic errors (such as in-common inaccuracies in foreground models) could be larger. We adopt the spread of all the curves as an estimate of the systematic error.

4. RESULTS

An important result of this analysis is to demonstrate the remarkable agreement between $C(\Theta)$ calculated from the WMAP and *Planck* maps of the CMB sky over a large range of Θ . The agreement is significantly better than was apparent from previously published plots and is the result of a uniform analysis.

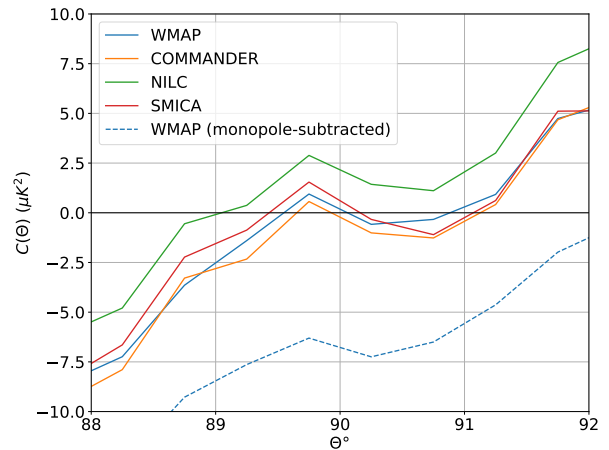


Figure 3. A closer view of $C(\Theta)$ near $\Theta = 90^\circ$ made with no masks. SEVEM lies outside the range of this plot. The other *Planck* maps span a total range of less than $3\mu K^2$. The agreement between the WMAP, SMICA and Commander maps is exceptional, with total range at 90° of only $0.83\mu K^2$. The dotted line shows $C(\Theta)$ for the monopole- and dipole-subtracted WMAP ILC map.

4.1. Correlation Function at 90 Degrees

The results illustrated in Figs. 2 and 3 show that over a range of Θ near 90° , the differences in measured $C(\Theta)$ from instrument and scan strategy systematics and statistical errors in the measurements are small compared to errors introduced by independent foreground subtraction, which are in turn small compared to errors known to be introduced by masking.

Our most striking new result is that there is general agreement on a very small absolute value of C_{90} in WMAP and *Planck* maps analyzed with no mask. All of the maps show this result except one outlier, SEVEM, which can be excluded due to residual foreground contamination. The range spanned by the other three *Planck* maps is $-0.22\mu K^2 < C_{90} < +2.16\mu K^2$. Combining these with the monopole-subtracted WMAP, the lower end of the range extends to $-6.7\mu K^2$. Although it is possible that an in-common foreground subtraction error between the different schemes perfectly cancels a nonzero primordial signal, the best overall estimate is consistent with a value of C_{90} very close to zero.

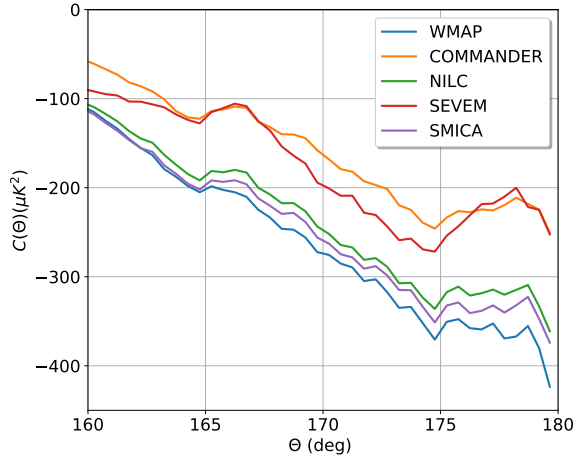


Figure 4. Plots of $C(\Theta)$ for the five unmasked maps at $\Theta > 160^\circ$.

4.2. Correlation Function Above 160 Degrees

At large angles $\Theta > 160^\circ$, the differences among the maps are much larger than at 90° . All of the maps show a similar shape, a significant negative correlation and a significant negative slope, but differ in magnitude by nearly a factor of two (Fig. 4). The differences in foreground modeling appear to have a larger effect than systematic bias produced by masking, in contrast to the situation near 90° . Some but not all of the difference can be accounted for by contributions $\delta C_1(\Theta) \propto \cos(\Theta)$ due to unsubtracted dipole components, which vanish for some but not all of the maps.

5. INTERPRETATION

Standard inflation theory predicts an ensemble of possible correlation functions. For the actual sky, which is just one realization, this leads to a large range of possible values of $C(\Theta)$, due to the cosmic variance of fundamentally independent modes. The standard interpretation is that the specific measured value of $C(\Theta)$ has little particular significance, since it is just one realization. Even so, as previously noted (Bennett et al. 2003, 2011; Schwarz et al. 2016; Ade et al. 2016; Akrami et al. 2019) and as shown in Fig. 5, measured values of $C(\Theta)$ depart significantly from those expected in the standard picture.

Holographic inflation predicts that there should be universal correlation properties in the angular domain. In this model, some specific features of large angle relationships, such as $C_{90} = 0$, can be understood as predictable consequences of holographic symmetries of a quantum-geometrical horizon wave function, rather than as statistical flukes in a random ensemble (Hogan 2019b). This kind of global, nonlocal connection between large- ℓ and large- Θ properties appears to violate

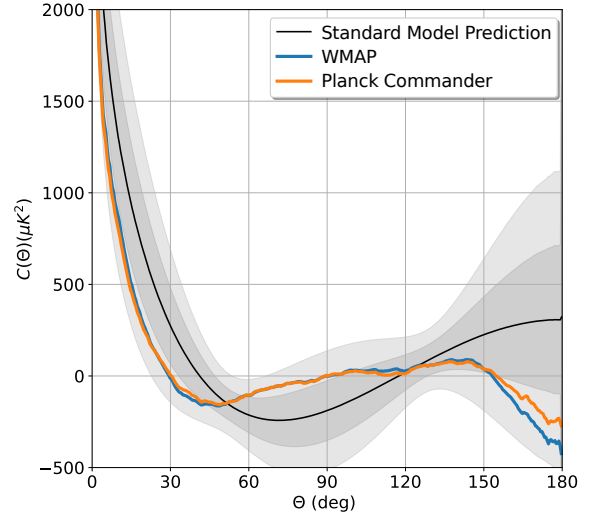


Figure 5. Comparison of the unmasked WMAP and *Planck* Commander correlation functions. Also shown as a black line is the mean, the 65% (dark band) and 95% (lighter band) range of $C(\Theta)$ calculated from an ensemble of sky maps made using predictions of standard quantum inflation.

statistical homogeneity and isotropy in the standard picture, but in holographic inflation, they arise from the emergence of the local rest frame and global metric from quantum relationships with any observer based on covariant causal diamonds that have no preferred velocity or direction, and entangle structure on all scales and directions. Simply put, *holographic causal symmetries in the angular domain appear to be miraculous in the natural harmonic basis of the standard scenario.*

The difference between these scenarios becomes significant if theory is compared with specific, precisely determined values. To illustrate this point with the current analysis, consider the nearly-null value of $C(\Theta)$ at 90° shown in Fig. 3, compared with the large range $> 300\mu K^2$ of predicted values from standard quantum inflation, as shown in Fig. 5. In the standard picture, the close agreement with zero found in the sky at 90° would be spoiled by 1σ variations of even a few of the hundreds of harmonic power coefficients (C_ℓ 's) at the map resolution. For example, 0.52% of standard realizations produce C_{90} by chance in the range spanned by SMICA, WMAP, Commander and NILC ($-0.22\mu K^2 < C_{90} < +2.16\mu K^2$). A larger fraction (1.5%) falls within the larger range also encompassed by the monopole-subtracted WMAP. If an additional constraint is added at $\Theta = 30^\circ$ using the range of measured values, $-20\mu K^2 < C(30^\circ) < +17\mu K^2$, only one out of 12,813 standard-model realizations agrees with both constraints. A holographic model could produce

$C(\Theta) = 0$ at these angles by symmetry, consistent with both constraints.

Another, less precise example is the increasingly negative correlation found at separations $\Theta > 160^\circ$, which confirms the odd-parity power asymmetry previously found via harmonic analysis (Ade et al. 2016; Akrami et al. 2019) to be anomalous in the standard picture at the 0.2% level for ℓ up to about 30. Both results show that opposite points on the sky tend to have opposite values, even at a resolution of a few degrees.

6. CONCLUSION

Our analysis shows overall consistency between independent measurements by different satellites, and among several independently developed foreground subtraction schemes. We show that better estimates of $C(\Theta)$ are likely possible with existing data, which may be used to test new quantum models of inflation. We defer a more detailed comparative likelihood analysis of quantum inflation models to future work that incorporates more detailed attention to effects of foreground models.

In the future, improved measurements of polarization, especially all-sky polarization maps with more comprehensive spectral information, should enable better separation of the primordial pattern of scalar curvature on

the horizon from other cosmological and astrophysical sources of anisotropy. It may also be possible to measure holographic directional correlations of primordial curvature in the pattern of 3D large scale structure, with sufficiently large and complete galaxy surveys.

ACKNOWLEDGMENTS

This work was supported by the Fermi National Accelerator Laboratory (Fermilab), a U.S. Department of Energy, Office of Science, HEP User Facility, managed by Fermi Research Alliance, LLC (FRA), acting under Contract No. DE-AC02-07CH11359, and by a National Science Foundation REU program at the University of Chicago. We acknowledge the use of HEALPix/healpy and the Legacy Archive for Microwave Background Data Analysis (LAMBDA), part of the High Energy Astrophysics Science Archive Center (HEASARC); the NASA/ IPAC Infrared Science Archive, which is operated by the Jet Propulsion Laboratory, California Institute of Technology, under contract with the National Aeronautics and Space Administration; and UTSA's SHAMU and UA's Ocelote HPC clusters. We are grateful to the referee for helpful comments.

REFERENCES

- Ade, P. A. R., et al. 2016, *Astron. Astrophys.*, 594, A16
- Akrami, Y., et al. 2018, *A&A*, arXiv:1807.06205
- . 2019, *A&A*, arXiv:1906.02552
- Banks, T., & Fischler, W. 2018, *Int. J. Mod. Phys.*, D27, 1846005
- Bennett, C. L., Halpern, M., Hinshaw, G., et al. 2003, *The Astrophysical Journal Supplement Series*, 148, 1
- Bennett, C. L., Hill, R. S., Hinshaw, G., et al. 2011, *The Astrophysical Journal Supplement Series*, 192, 17
- Bennett, C. L., Larson, D., Weiland, J. L., et al. 2013, *The Astrophysical Journal Supplement Series*, 208, 20
- Gorski, K., Hivon, E., Banday, A., et al. 2004, *apj*, 622, doi:10.1086/427976
- Hogan, C. 2019a, *Phys. Rev. D*, 99, 063531
- . 2019b, arXiv:1908.07033
- Hogan, C. J. 2017, *Phys. Rev. D*, 95, 104050
- Hogan, C. J., Kwon, O., & Richardson, J. 2017, *Class. Quantum Grav.*, 34, 135006
- Jacobson, T. 1995, *Phys. Rev. Lett.*, 75, 1260
- . 2016, *Phys. Rev. Lett.*, 116, 201101
- Natsuume, M. 2015, *Lect. Notes Phys.*, 903, pp.1
- Padmanabhan, T. 2014, *Gen. Rel. Grav.*, 46, 1673
- Planck Collaboration. 2014, *A&A*, 571, A12
- . 2016a, *A&A*, 594, A9
- . 2016b, *A&A*, 594, A10
- Ryu, S., & Takayanagi, T. 2006a, *JHEP*, 08, 045
- . 2006b, *Phys. Rev. Lett.*, 96, 181602
- Schwarz, D. J., Copi, C. J., Huterer, D., & Starkman, G. D. 2016, *Class. Quant. Grav.*, 33, 184001
- Solodukhin, S. N. 2011, *Living Rev. Rel.*, 14, 8
- 't Hooft, G. 2016a, *Found. Phys.*, 46, 1185
- . 2016b, arXiv:1605.05119
- . 2018, *Foundations of Physics*, 48, 1134
- Verlinde, E. P., & Zurek, K. M. 2019, arXiv:1902.08207